Fire Safety Journal 141 (2023) 103883

Contents lists available at ScienceDirect

Fire Safety Journal

journal homepage: www.elsevier.com/locate/firesaf

Optimising the inherent fire capacity of structures

Andrea Franchini *, Carmine Galasso, Jose L. Torero

University College London, Gower St, London, UK

ARTICLE INFO

Keywords:
Fire safety
Structural engineering
Optimisation
Probabilistic design
Passive protection
Inherent capacity

ABSTRACT

This paper introduces a structural design optimisation methodology aimed at minimising the consequences of a fire. The methodology considers the trade-off between implementing passive fire protection measures and enhancing a structure's "inherent fire capacity", defined as its ability to retain integrity/functionality without additional fire safety measures. The feasibility of the methodology is demonstrated through the fire safety design of a single-span, steel girder bridge. The optimisation process generates multiple Pareto-optimal solutions for minimising the maximum bridge deflection after a given fire exposure time. Passive protection ensures the bridge's functionality when facing a heavy goods vehicle fire. In the case of exposure to a car fire, solutions requiring fire protection in specific limited girder regions are identified. The decision-making process is further supported by investigating the robustness of the solutions to uncertainties in material properties and the heat flux model.

1. Introduction

Performance-based structural fire engineering is gaining widespread acceptance in the field of fire-safety design. In this respect, both deterministic (e.g. [1,2]) and probabilistic (e.g. [3,4]) approaches have been proposed and implemented. These approaches can be used to either *assess* proposed structural designs/existing structures (i.e. test their adequacy in terms of target performance objectives) or *design* new structures, including fire considerations (i.e. select the geometry, materials, structural layout and fire safety strategy to achieve desired performance objectives). This paper focuses on the latter aspect.

Most existing design approaches rely upon preliminary assumptions on the structural configuration and features characterising scenarios used as thermal inputs. This approach, proven highly effective for other hazard types such as earthquakes or extreme wind, might not be optimal for fire safety design. Indeed, the strong coupling between the fire phenomenon and structural features enables an ad-hoc design variable selection (and/or optimisation) to reduce fire intensity, making fire scenarios additional design outputs.

In this respect, Torero [5,6] highlighted that structural and fire behaviour are dynamically coupled, resulting in a fire-structure coupling effect where the fire dynamics change as a consequence of the structural configuration and responses and vice-versa. This dependence further implies that fire scenarios maximising consequences are structure-specific.

Embracing these unique features of fire hazard, Franchini et al. [7] have recently developed an alternative methodology to fire safety design called the Consequence-oriented Fire Intensity Optimisation (CFO) approach. The method exploits the coupled influence that a structure and fire dynamics have on each other for an ad-hoc *(structural) design variable selection* that reduces fire intensity until rendering maximum fire consequences compliant with given performance objectives.

The methodology can be further developed to minimise maximum fire consequences through *design variable optimisation*. Such variables include passive fire protection measures that rely on built-in features to prevent fire spread and protect structural integrity [8].

However, implementing passive fire protection measures can present challenges and necessitates solving trade-offs. Indeed, these measures may lead to uneconomical designs, with fire protection accounting for a significant portion of structural costs, such as in steel buildings [9]. Additionally, applying insulating materials on bridge structures can be expensive and demands continuous maintenance [10,11]. This maintenance is generally required for passive measures, which can be susceptible to ageing and partial loss [12].

To address these issues, there is a growing interest in investigating the inherent fire resistance of structures. Enhancing the inherent fire resistance of unprotected structures can lead to more efficient and cost-effective designs [10]. The concept of "inherent resistance" refers to a structure's fire resistance without relying on any additional fire protection measures. Buchanan and Abu [8] discussed a similar concept, stating that a better understanding of fire and structural behaviour enables designers to exploit the "fire resistance [...] inherent in buildings due to their structural form". Such resistance was observed, for example, in the excellent performance of unprotected elements during the Building Research Establishment (BRE) Cardington fire test [13]

* Corresponding author.
E-mail addresses: andrea.franchini.19@ucl.ac.uk (A. Franchini), c.galasso@ucl.ac.uk (C. Galasso), j.torero@ucl.ac.uk (J.L. Torero).

https://doi.org/10.1016/j.firesaf.2023.103883
Received 10 June 2023; Accepted 24 July 2023
Available online 26 July 2023

(due to membrane actions). The idea of inherent fire resistance aligns with the "inherently safer" design philosophy proposed by Kletz and Amyotte [14]. When applied to fire engineering, such a philosophy implies enhancing the inherent fire performance of a structure, i.e. its resistance without safety measures [15]. Given these premises, the objectives of this paper are to:

- Develop a CFO-driven design optimisation methodology to minimise the (maximum) consequences of a fire.
- Within such a methodology, address the trade-off between implementing passive fire protection (e.g. fireproof layers on steel cross-sections) and enhancing the "inherent fire capacity" of the structure – that is, its capacity to retain its integrity/functionality without fire protection.
- Showcase the methodology applicability through the fire safety design of a simple case study structure. To this aim, a single-span, steel girder bridge is considered.
- In the context of the case study, implement a simplified stochastic model for the heat transfer from the flames to the bridge that is calibrated on experimental data and fundamentals of flame physics.

The remainder of the paper is organised as follows. Section 2 introduces the proposed optimisation methodology and formally defines the inherent fire capacity. An illustrative case study is presented in Section 3, and conclusions are drawn in Section 4.

2. Proposed methodology

2.1. Minimising maximum fire consequences

The CFO approach [7] was developed as a tool to identify design solutions that optimise fire intensity (and the associated consequences) through comparative assessment. This paper proposes using the CFO approach to minimise maximum fire consequences.

The methodology is shown in Fig. 1. It starts by defining the fire safety performance objectives to optimise (step I), including life safety, property protection, continuity of operations and environmental protection [16]. In step II, a consequence potential model, $CP(\mathbf{X}, \mathbf{X}_{strat}, \boldsymbol{\alpha})$, is developed to quantify the potential for fire-induced consequences as a function of structural and fire safety strategy design variables $(\mathbf{X}, \mathbf{X}_{strat})$ and fire modelling characteristics $\boldsymbol{\alpha}$ not included in the former two variable sets (e.g. fuel bed position, fuel load). Step III ("consequence maximisation") uses the CP and numerical optimisation techniques to determine the maximum consequence potential MC and the corresponding fire scenario $\boldsymbol{\alpha}_{MC}$ (within the considered structural context). For a given design variable combination, maximum consequences are obtained as follows:

$$\mathbf{X} = \mathbf{X}', \mathbf{X}_{strat} = \mathbf{X}'_{strat} \rightarrow MC, \boldsymbol{\alpha}_{MC} = max\{CP(\boldsymbol{\alpha})\} \tag{1}$$

An additional optimisation cycle (step IV, "Maximum consequence minimisation" in Fig. 1) is then applied to find design variables $\mathbf{X}^*, \mathbf{X}^*_{strat}$ that minimise MC:

$$MC_{min}, \mathbf{X}^*, \mathbf{X}^*_{strat} = min\left\{MC\left(\mathbf{X}, \mathbf{X}_{strat}\right)\right\} \tag{2}$$

Solving Eq. (2) requires the results of Eq. (1) at each iteration. The minimum MC calculation aligns well with the recommendation of designing structures to obtain a "minimum (fire) damage potential" as an alternative to the use of design fires [5].

Thus far, the described methodology is deterministic as advocated by various studies on consequence assessment (e.g. [14,15,17,18]). However, input uncertainties (such as those related to material properties, structural component geometry, and models) make the optimal maximum consequence potential a random variable $\overline{MC}_{min}$. Therefore, step V investigates the unknown distribution of this variable through Monte Carlo sampling. The purpose of this analysis is to assess the the solution's robustness to uncertainties (i.e. its limited sensitivity to input variations) and to estimate the probability of not achieving the performance objectives. Robustness can be quantified through dispersion statistics (e.g. the coefficient of variation, CoV, of $\overline{MC}_{min}$, obtained as the ratio of the standard deviation to the mean).

The calculated consequence metrics inform decision making in step VI. Due to the large number of design criteria that a structure needs to satisfy (e.g. functionality, safety, sustainability, cost), the maximum consequence optimisation might provide several optimal solutions that prioritise some criteria over others. This overall methodology is especially pertinent when dealing with structures that are complex and/or entail significant consequences if lost.

2.2. Inherent fire capacity optimisation

The recent literature (e.g. [8,10,13–15]) indicates the existence of an inherent resistance in structures exposed to fire. Still, to the authors' knowledge, a formal definition of this concept has not been established, which hinders its widespread exploitation for design. Therefore, this paper seeks to fill this gap by introducing an explicit definition. The term "inherent fire capacity" is suggested to describe a structure's capacity to retain its integrity/functionality without the need for additional fire safety measures (active and passive protection).

The term "fire resistance" is not deemed suitable for capturing this concept as it is already associated with the minimum duration for which a structural element or component meets insulation (I), integrity (E), and load-bearing capacity (R) requirements during standard furnace testing [8,12,19]. Therefore, the proposed terminology of "inherent fire capacity" encompasses the structural fire performance in a broader sense without relying on supplementary fire safety measures.

The calculation of MC in Eq. (1) refers to a fixed set of design variables. When active fire protection measures are not included in the fire safety strategy, MC can be viewed as a function of the structure's inherent fire capacity (IC) and the additional capacity provided by passive fire protection (protected capacity, PC):

$$MC = f(IC, PC) \tag{3}$$

Hence, solving Eq. (2) implies that different combinations of IC and PC can lead to the same MC_{min}. Consequently, a trade-off exists between these two capacities, and the optimal level of IC needs to be determined on a case-by-case basis. As discussed in Section 1, the decision to prioritise IC over PC may be influenced by factors such as cost-effectiveness, the practicality of implementing specific passive fire protection measures, and potential maintenance requirements.

The following section demonstrates the implementation of the proposed methodology for the fire safety design of a case study bridge. In this example, several simplifying assumptions are drawn, especially concerning the structural and fire models. For a comprehensive discussion of these simplifications, the reader is referred to Appendix I of Franchini et al. [7]. The primary objective here is to illustrate the proposed methodology rather than generate "definite" results.

3. Illustrative example

3.1. Case study description

The single-span bridge studied by Peris-Sayol et al. [20] (with the simplifying assumptions from Ref. [7]) and illustrated in Fig. 2 is considered in this section. The bridge has a vertical clearance $H_{\#1}$ = 5.00 m and is made of five W36x300 girders with height $H_{\#1,gir}$ = 0.91 m, flange width $w_{f,\#1}$ = 0.424 m and span L_{gir} = 21.34 m. The subscript "#1" identifies the initial design configuration. The girders, which support a 0.20 m concrete slab, are made of steel with a yielding stress of 250 MPa and elastic modulus E = 210 GPa. Only the central girder is considered in this paper and a 2D analysis in the x–y plane (shown in the figure) is conducted.

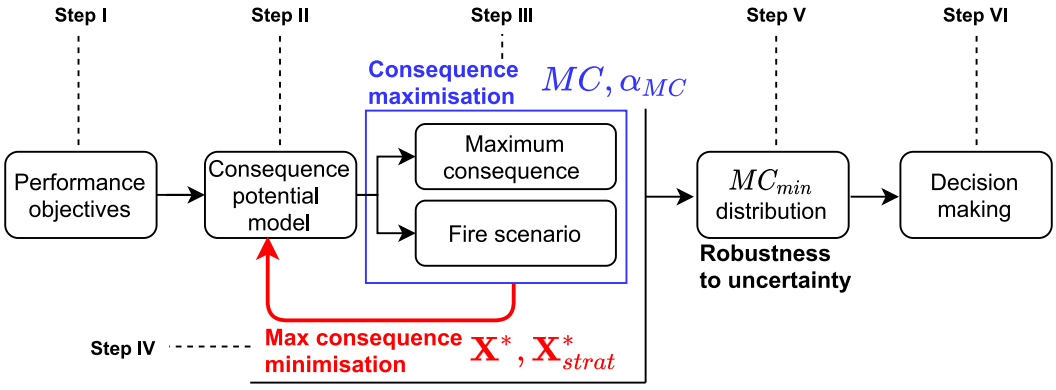

Fig. 1. CFO (Consequence-oriented Fire Intensity Optimisation) -based maximum fire consequence minimisation.

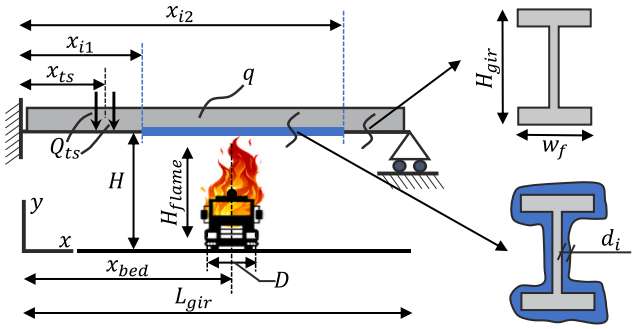

Fig. 2. Case study bridge. Symbols: L_{gir} girder length; x_{bed} fuel bed location; D fuel bed diameter; H bridge clearance; H_{flame} mean height of the flame plume; x_{ts} tandem system location; Q_{ts} concentrated loads (tandem system); x_{i1}, x_{i2} starting and finishing locations of the insulation layer; q uniformly distributed load; H_{gir} girder height; w_f flange width; d_i thickness of the insulation layer.

A fixed end constraint is assumed on the left-hand side of the girder (see Fig. 2) to demonstrate the proposed methodology's capability of identifying fire scenarios maximising consequences and treating such scenarios as additional design variables. Another difference with respect to the reference is the consideration of a passive fire protection layer of thickness d_i that insulates the girder in the $[x_{i1}, x_{i2}]$ interval. The insulation consists of sprayed mineral fibre with density $\rho_i = 300$ kg/m^3, thermal conductivity $k_i = 0.12$ W/m K and specific heat $c_i = 1200$ J/kg K [8].

The effect of traffic is modelled through a uniformly distributed load $q_1 = \alpha_{q1} \times 9$ kN/m^2 and two double axle concentrated loads (tandem system) $Q_{ts} = \alpha_{Q1} \times 300$ kN (Load Model 1, Notional Lane 1 [21]). α_{q1} and α_{Q1} are adjustment factors (assumed equal to 0.8, which is the minimum value recommended by the Eurocode). The tandem system is located at $x_{ts} = \alpha_{ts} \times L_{gir}$ from the origin. Here, L_{gir} is the girder length, and α_{ts} is a general scaling factor that is to be determined to maximise consequences. Following these considerations, the load q in Fig. 2 consists of the sum of the girder's dead load, the superimposed dead load of the slab and bridge pavement, and q_1 described above.

The fire scenario involves a localised vehicle fire positioned at $x_{bed} = \alpha_{bed} \times L_{gir}$. Numerical optimisation (step III in Fig. 1) will be employed to determine the burning vehicle location, the tandem system location, and the fire model properties maximising consequences.

Six bridge design variables are selected to achieve the performance objectives: the vertical clearance H; the girder depth H_{gir}; the flange width w_f; the thickness of the insulation layer d_i; and the starting and finishing locations (x_{i1}, x_{i2}) of the insulation layer. Increasing H reduces the heat flux to the girder. However, selecting this design variable requires careful consideration. Indeed, its modification implies adjusting the abutment and the approach height through additional earthworks. Thus, this paper assumes that stakeholders/designers could account for these issues to better optimise the balance between IC and PC. A low section factor (ratio of heated perimeter to the cross-sectional area [8]) slows down the temperature rise in a fire exposed girder. The factor can be altered by modifying H_{gir} and w_f. From a thermomechanical perspective, these two variables modify the girder moment of inertia and its bearing capacity. Finally, the insulation layer reduces the heat flux to the protected sections of the girder. The design variable vector can then be defined as follows:

$$\mathbf{X} = \left[X_H, X_{Hgir}, X_{wf}, d_i, X_{xi1}, X_{xi2}\right] \tag{4}$$

In this equation, X_H, X_{Hgir}, X_{wf} are multiplicative factors for the corresponding properties in the initial design configuration; d_i is the fire protection thickness; $X_{xi1}, X_{xi2} \in [0, 1]$ are multiplicative factors such that $x_{i1} = X_{xi1} L_{gir}$ and $x_{i2} = X_{xi2} L_{gir}$.

3.2. Performance objectives

The selected performance objective is for the considered bridge to maintain its functionality (and, therefore, integrity) for 60 min when exposed to a vehicle fire. This specific value is selected based on the duration of past bridge fires [10], but the proposed approach is general and can use any predefined performance objective. A car fire and a heavy goods vehicle (HGV) fire are considered for comparative purposes. Four post-fire damage states are defined based on the maximum girder deflection δ_{max} during the fire event [22]: superficial damage ($\delta_{max} \leq L_{gir}/160$); moderate damage ($L_{gir}/160 < \delta_{max} \leq L_{gir}/80$); heavy damage ($L_{gir}/80 < \delta_{max} \leq L_{gir}/20$); and hazardous damage ($\delta_{max} > L_{gir}/20$).

Here, it is assumed that functionality is maintained if the structure remains in the superficial damage state (for the specified period). The performance objective is to be achieved by optimising the balance between inherent and protected fire capacity (IC and PC). Furthermore, the solution's robustness to input uncertainty is to be assessed.

3.3. Consequence potential model

3.3.1. Heat release rate

The vehicle fire is modelled through a bilinear heat release rate (HRR) function representing the time history $HRR(t)$ of the amount of energy released by the fire. The HRR starts at the ignition time and grows linearly up to a peak value hrr_{max}, which is reached at the time t_{max}. Then, the curve remains constant until burnout (t_{bo}). The total energy the burning vehicle releases, named ER, is obtained

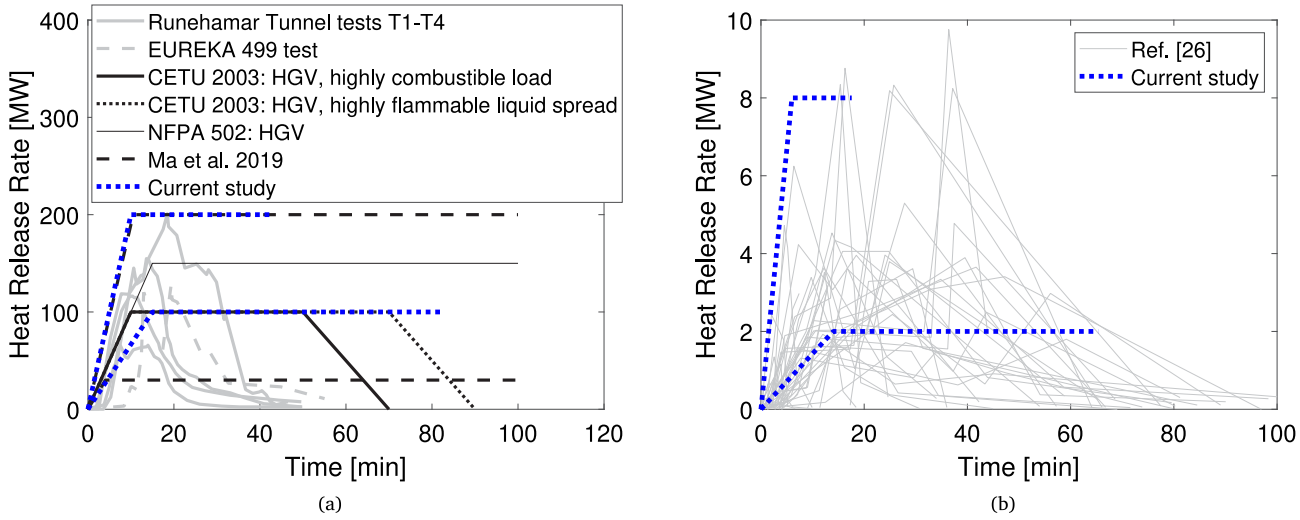

Fig. 3. Reference heat release rate time histories for: (a) heavy goods vehicle (HGV) fire; (b) car fire.

Table 1
Heat release rates.

Variable	Car fire	HGV fire
ER [GJ]	7	450
hrr_{max} [MW]	2–8	100–200
t_{max} [min]	6–14	10–15

by integrating $HRR(t)$ over time. For a fixed ER value, different combinations of hrr_{max} and t_{max} result in different HRR time histories, spanning from a short-hot to a long-cool fire.

The selected parameters should be representative of real vehicle fires. For HGVs, experimental data from the Runehamar tunnel test and the EUREKA test [23] are compared to the models recommended by the National Fire Protection Association (NFPA 502; [24]), Centre d'Études des Tunnels (CETU; [25]) and Ma et al. [4] (Fig. 3a).

On the other hand, for the car fire, the experimental data reported by Mohd Tohir and Spearpoint [26] are considered (see Fig. 3b). This analysis provides the HRR modelling parameters summarised in Table 1. For the selected value of ER, the two parameters $hrr_{max} = \alpha_{hrrmax} \times hrr_{max,ref}$ and $t_{max} = \alpha_{tmax} \times t_{max,ref}$ describe a general HRR curve. Here, α_{hrrmax} and α_{tmax} are multiplicative factors, while $hrr_{max,ref}$ and $t_{max,ref}$ are the average values of the ranges from Table 1. Finally, a vector of fire scenario features is defined as $\boldsymbol{\alpha} = [\alpha_{bed}, \alpha_{hrrmax}, \alpha_{tmax}, \alpha_{ts}]$. Fig. 3 shows the selected HRR curve ranges. These curves are adopted in the next section to calculate heat fluxes to the girder.

3.3.2. Heat flux

The heat release rate is given by the product of the heat of combustion ΔH_c, the burning rate per unit area $\dot{m}''$, and the area of the fuel A_f (i.e. $HRR = \Delta H_c \dot{m}'' A_f$). The burning rate can be expressed as follows:

$$\dot{m}'' = \frac{\dot{q}''_{flame} + \dot{q}''_{feedback} - \dot{q}''_{loss}}{L_V} \tag{5}$$

where $\dot{q}''_{flame}$ is the heat flux supplied by the flame; $\dot{q}''_{feedback}$ is the heat feedback from the environment to the fuel bed; $\dot{q}''_{loss}$ is the heat loss from the fuel surface; L_V is the heat required to gasify the fuel [27]. Eq. (5) shows that the burning rate is influenced by the heat feedback from the environment surrounding the fire. Since the heat flux to the girder depends on the heat release rate (and therefore on the burning rate), this section attempts to capture this correlation.

Turbulent, buoyancy-driven diffusion flames are usually of interest in the context of bridge fires. The nature and dynamics of the fire plume interacting with the bridge deck determine the heat flux from the fire to the girder. McCaffrey [28] showed that the fire plume consists of three regimes (Fig. 4a): persistent flame zone, intermittent flame zone, and buoyant plume. The author also provided experimental correlations for the flame centreline excess temperature ΔT in the three zones. The first two zones can be jointly addressed as "flame plume" (e.g. [29]). Many studies have followed the work of McCaffrey, reaching similar descriptions, and are summarised in the Society of Fire Protection Engineers (SFPE) Handbook [30].

As schematically depicted in Fig. 4b, average temperatures increase for distances up to 10% of the flame height. Then, they remain relatively constant for distances up to 40%–50% of the flame height before decreasing towards the flame tip [28,31]. A similar trend is therefore expected for the heat flux $\dot{q}''_f$ from the fire to an object immersed in or impinged by the fire plume. Hence, the heat flux can be correlated to a curvilinear abscissa s that starts at the fuel bed and moves along the flame centreline (see Fig. 4a).

The mean height of the flame plume is defined as the distance above the fire source where the intermittency equals 0.5 [30]. Such a height can be estimated based on experimental studies from Heskestad [32]:

$$H_{flame}(t) = 0.235\,(HRR(t))^{2/5} - 1.02D \tag{6}$$

where t is the time, and D the (equivalent) diameter of the fuel bed. At each time step, H_{flame} is compared to the bridge clearance H to determine whether the flame plume impinges on the deck.

If the flame plume does not impinge ($H_{flame} < H$; Fig. 4c), Alpert's correlations [33] are used to calculate the maximum ceiling jet excess temperatures and the convective heat flux to the girder. Additionally, the radiative heat flux from the flame plume is computed through the point source model [34]. If only the buoyant plume impinges on the deck ($H_{flame} < H$), the heat feedback $\dot{q}''_{feedback}$ to the fuel bed is negligible with respect to $\dot{q}''_{flame}$.

The heat flux increases drastically in the case of flame plume impingement ($H_{flame} \geq H$; Fig. 4d–e). In this case, the heat feedback $\dot{q}''_{feedback}$ might significantly affect the combustion process by increasing the burning rate. For instance, an increased burning rate was measured in the Valencia bridge fire test [35,36] when the burning pan was moved closer to the deck. Furthermore, several other factors affect $\dot{q}''_f$, including the confining effect of girders and stiffeners on the ceiling jet flow, environmental conditions, and structural surfaces' nature and geometry.

This paper implements a simplified heat flux model for impinging flame plumes – calibrated on experimental data – to capture such

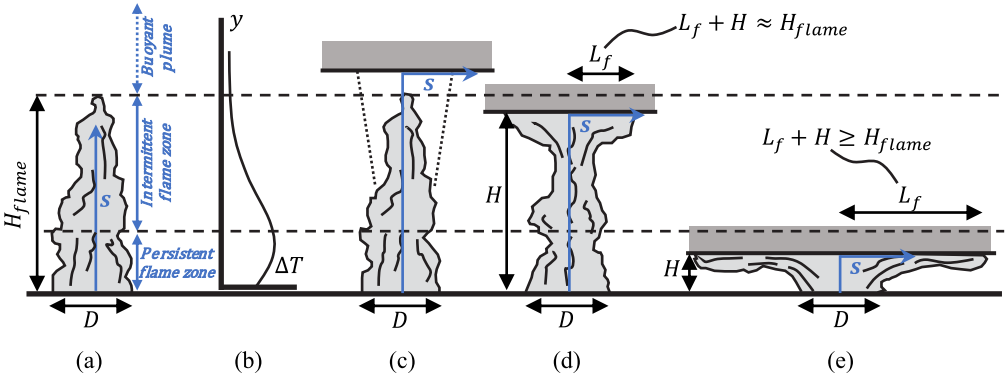

Fig. 4. Fire plume and its interaction with the bridge deck. Symbols: s curvilinear abscissa; D fuel bed diameter; H bridge clearance; H_{flame} mean height of the flame plume; ΔT centreline excess temperature; L_f horizontal flame length.

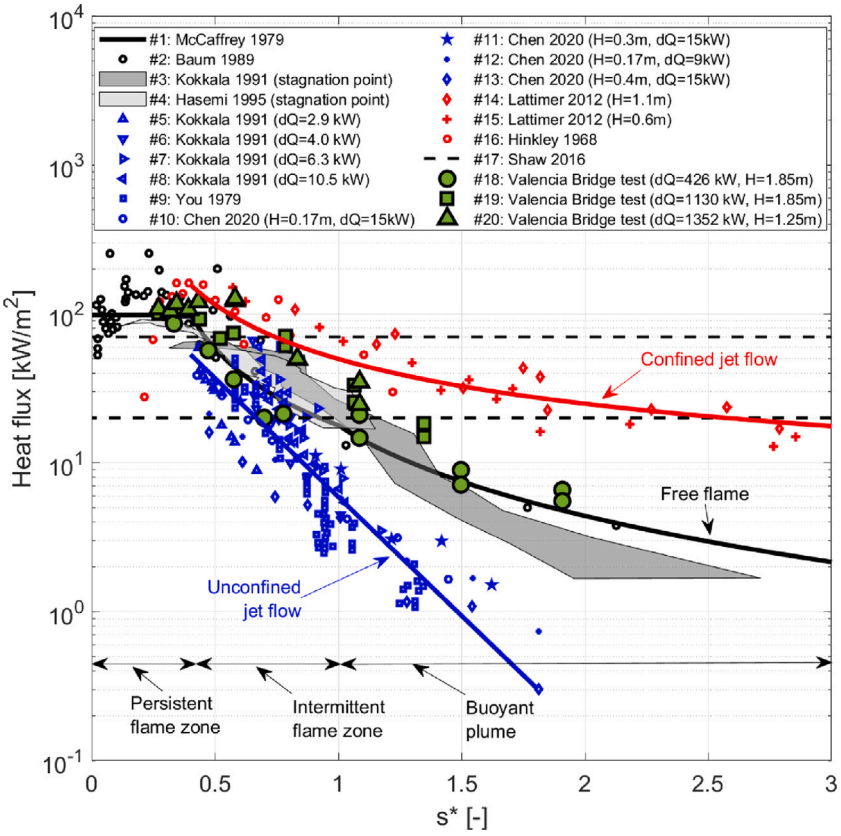

Fig. 5. Experimental data for the heat flux as a function of the nondimensional abscissa s^* and fitted curves. (For interpretation of the references to colour in this figure legend, the reader is referred to the web version of this article.)

factors. The data were retrieved from studies in the literature, which are listed in Table A.1 of the Appendix. They include heat flux or centreline temperature measurements obtained in different contexts: free flames [28,37]; unconfined ceilings [29,38,39]; confined ceilings [40,41]; tunnel fires [42,43]; bridge fires [36]; and objects immersed in large pool fires [44]. The scope of the analysis was to capture how the heat flux correlates with the curvilinear abscissa s in different configurations (e.g. confined or unconfined gas flow) and with the impingement zone (continuous or intermittent flame zone).

As shown in the third column of Table A.1, data from different references were presented in different formats (e.g. centreline excess temperature, nondimensional heat flux) and as functions of different problem length scales (e.g. mean flame length, flame tip length, distance along the ceiling from the impingement point). Therefore, the joint analysis of all the data required the scaling assumptions listed in the fourth column of Table A.1. The data are plotted in Fig. 5 as a function of the nondimensional abscissa s^*:

$$s^* = \frac{s + y_0}{H_{flame} + y_0} \tag{7}$$

where $y_0 = 0.083\dot{Q}^{2/5} - 1.02D$ is the virtual source location [30]. When heat flux data refer to the impingement point at a distance H from the fuel bed, $s = H$. Differently, if the heat flux is given as a function of the distance r from the impingement point, $s = r + H$. The main observations from Fig. 5 are the following:

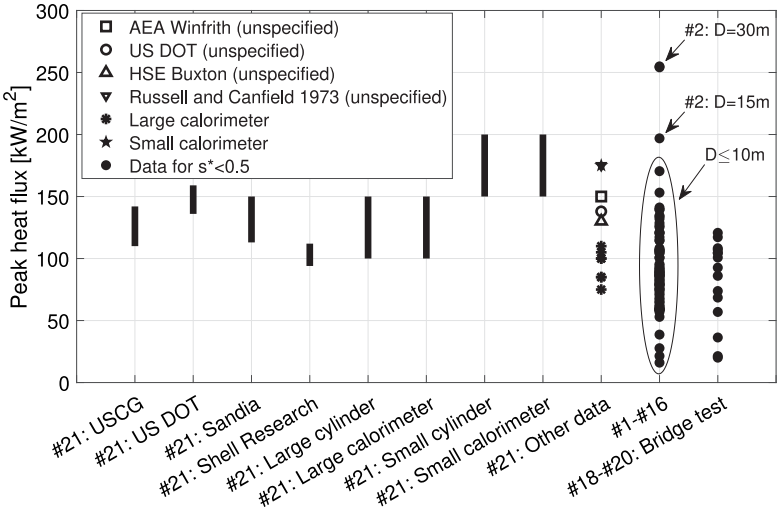

Fig. 6. Experimental data for the peak heat flux. Symbols: s^* nondimensional abscissa; D pool diameter.

- The data cluster around three different regimes: unconfined jet flow, free flame, and confined jet flow.
- The heat flux attains its maximum value if the ceiling deflects the persistent flame zone, whereas it decreases if the impingement occurs at the intermittent flame zone. This is consistent with the centreline flame temperature trend described by McCaffrey [28].
- The trend of heat flux measurements at the stagnation point (#3, #4, and the initial points of #5 to #16) is well represented by the free flame regime. However, for increasing s^*, the heat flux deviates from the free flame: it decreases in an unconfined jet flow and increases in a confined one. This fact is motivated by the different air entrainment in the three regimes.
- The results of the Valencia bridge fire test (green markers in Fig. 5) suggest that the heat flux to a real girder bridge is between the two regimes. The free flame regime represents the heat flux well for limited flame impingement (data #18). As H/H_{flame} reduces, the behaviour tends to the confined jet flow regime (data #19 and #20).

A statistical model for the heat flux is calibrated on the considered experimental data. Close to the pool surface (persistent flame zone), the heat flux is characterised by a uniform distribution $\mathcal{U}$. Fig. 6 compares heat flux measurements for objects immersed in large pool fires with the results of Fig. 5 in the persistent flame zone ($s^* \approx 0.0$–0.5). Cowley [45] discussed that the small-scale correlations for centreline temperature by McCaffrey [28] are also accurate for large-scale fires except in the persistent flame zone. Here, centreline temperatures in large pool fires are higher. This fact is reflected by the dataset #2 in Fig. 5, which refers to measurements on large pool fires by Baum and McCaffrey [37]. The data points for pool diameters equal to 30 m and 15 m are also highlighted in Fig. 6.

Equivalent diameters for car and track fires span between 2.8 m and 5.5 m [4]. Differently, the maximum size of a tanker fire (in the case of a fuel spill) depends on the characteristics of the lane. Assuming a lane of 4.5 m and a tanker length of 12 m, the equivalent diameter is 8.3 m. Based on these considerations and the data presented in Fig. 6, the uniform distribution boundaries are suggested in the range 100–150 kW/m^2.

Outside the persistent flame zone, the heat flux is assumed to be normally distributed and homoscedastic, with mean and standard deviation calibrated on the experimental data presented in Fig. 5 through linear regression. The results are summarised in Table 2. In this table: μ and σ represent the mean and the standard deviation of the normal distributions modelling the unconfined (subscript "unc") and confined (subscript "con") jet flow configurations; R^2 is the coefficient of determination, representing the goodness of fit of the regression model to the observed data. The boundary of the persistent flame zone, s^*_{lim}, is obtained as the intersection of the heat flux curves for the two regions.

Table 2
Heat flux model for flame plume impingement.

Zone	Persistent flame	Intermittent flame and buoyant plume	
Nondim. abscissa	$s^* \le s^*_{lim}$	$s^* > s^*_{lim}$	
Regime	(all)	Unconfined	Confined
Model	$\mathcal{U}(a,b)$	$\mathcal{N}(\mu_{unc},\sigma_{unc})$	$\mathcal{N}(\mu_{con},\sigma_{con})$
Mean	$(a+b)/2$	$\mu_{unc} = exp\{a - bs^*\}$	$\mu_{con} = exp\{a/(s^*)^b\}$
Parameter: a	100 kW/m^2	5.561	3.783
Parameter: b	150 kW/m^2	4.033	0.346
Standard deviation	–	9.78 kW/m^2	17.43 kW/m^2
Coeff. of determination	–	$R^2 = 0.779$	$R^2 = 0.884$

3.3.3. Thermomechanical analysis

The obtained heat flux is used as the boundary condition for the thermal response analysis, aiming to compute the temperature's time history in the girder. Assuming a constant temperature distribution across the section is acceptable for this calculation, and is representative of an intermediate case between restraint expansion-dominated and gradient-dominated problems [46]. Further limitations of this assumption are discussed in Ref. [7]. Under this hypothesis, the temperature development in the unprotected sections of the girder is obtained through the lumped thermal mass approach described by Quiel et al. [2]. A two-lumped thermal masses calculation approach is applied for protected sections instead. The insulation layer adsorbs the heat flux from the fire and transfers conductive heat to the girder.

The obtained temperature's time histories are used to compute the bridge's structural response through the OpenSees for fire software [47]. Specifically, the girder is modelled using displacement-based elements with thermo-mechanical fibre sections. Each fibre is assigned the uniaxial material *Steeel01Thermal* [47], which includes the temperature-dependent properties from EN 1993-1-2 [48]. The displacement history of each girder node is monitored during the thermomechanical analysis, which starts from the deformed configuration induced by dead and traffic loads. This procedure provides the CP (see Section 2), i.e. the maximum deflection δ_{max} of the girder at the reference time for a given fire scenario $\boldsymbol{\alpha}$ and design variable configuration $\mathbf{X}$.

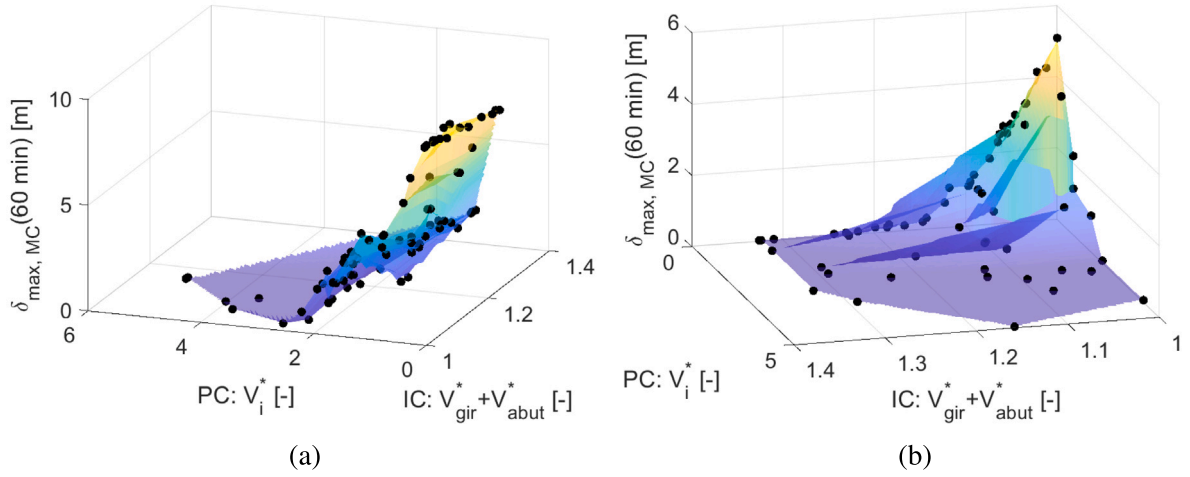

Fig. 7. Pareto front for: (a) HGV fire; (b) car fire.

3.4. Maximum consequence minimisation

The bilevel optimisation procedure described in Section 2 is applied to minimise the maximum deflection of the girder. The problem is addressed as a multiobjective optimisation to simultaneously minimise the maximum bridge deflection, the inherent and the protected capacity:

$$\mathbf{X}^{opt} = min\begin{bmatrix} \delta_{max,MC} \\ V^*_{gir} + V^*_{abut} \\ V^*_i \end{bmatrix} \tag{8}$$

In this equation: $\delta_{max,MC}$ is the maximum consequence potential, obtained at each iteration by solving the optimisation problem of Eq. (1); V^*_{gir} and V^*_{abut} are the ratio between the optimised girder and abutment volumes and their initial value; therefore, the sum of these two variables is a proxy for the IC of the structure; V^*_i is the ratio between the optimised fire protection volume and its initial value (assuming a 5 mm layer that covers the whole girder). Hence, V^*_i represents the PC of the bridge.

Solving Eq. (8) provides the Pareto fronts depicted in Fig. 7. The surfaces are obtained via linear regression. Each point corresponds to a Pareto-optimal solution, i.e. it optimises the trade-off between minimising the three performance metrics (maximum deflection, IC and PC). More precisely, in the context of multiobjective optimisation, a solution is defined as "Pareto-optimal" if one performance metric cannot be improved without degrading at least one of the other metrics [49]. It is observed that several cost metrics (e.g. initial, failure, or life-cycle cost) might also be considered as performance objectives or boundary conditions in the optimisation problem. Readers are referred to Franchini et al. [7] for an example.

The optimised deflections are compared to the deflection threshold described in Section 3.2 to assess the post-fire damage states. The results are reported in Fig. 8a,c. Design variable combinations corresponding to the Pareto-optimal points are displayed in Fig. 8b,d. Points laying on the horizontal axis of Fig. 8a,c represent solutions that rely solely on the inherent fire capacity. For HGV fires, ensuring the post-fire superficial damage state is not exceeded requires introducing fire protection over the entire length of the girder. This is evident from Fig. 8b, which shows that all design variable solutions achieving this performance are characterised by $X_{xi1} = 0$ and $X_{xi2} = 1$.

On the other hand, for car fires, the superficial damage state can be achieved without the requirement of PC, as indicated by the circles on the horizontal axis of Fig. 8c. In these cases, relying exclusively on the IC is sufficient. Intermediate solutions that involve partial protection of the girder length are observed in Fig. 8d, indicating that up to 40% of the girder length can be left unprotected while still limiting damage to the superficial state.

3.5. Robustness to uncertainty and decision making

For illustrative purposes, the three design configurations #1, #2, and #3 listed in Table 3 are selected from the configurations exhibiting superficial damage states for HGV fires. Design #1 represents the configuration with the lowest level of PC. In contrast, design #2 achieved the minimum deflection employing the largest amount of PC. Lastly, design #3 was chosen as an intermediate case.

Table 3 shows that the fuel bed and tandem system positions that maximise the girder deflection ($\alpha_{bed,MC}$, $\alpha_{ts,MC}$) differ among the three designs. Furthermore, these positions are not aligned in any of the cases. The HRR curves, represented by $\alpha_{hrrmax,MC}$ and $\alpha_{tmax,MC}$, also exhibit notable variations. In particular, the maximum consequences do not arise from the selected boundary conditions (i.e. short-hot or long-cool fire, see Fig. 3a). Instead, they are influenced by the specific characteristics of each design configuration. These findings emphasise that the fire scenarios resulting in the most severe consequences vary significantly across different design configurations.

Plain Monte Carlo sampling is adopted to estimate the probability that a selected design does not exceed the superficial damage state (representing the functionality performance objective in this study) due to uncertainty in the steel material properties and in the heat flux model. Table 4 [50] presents the material random variables and their probability models. Refer to Table 2 for the heat flux distributions. The probability of exceeding the considered damage state is denoted as p_f and estimated through 10^5 simulations. Design #2 emerges as the most reliable solution when the fire protection material volume (a proxy for the insulation cost) is not a primary concern. On the other hand, Design #1 requires the least fire protection, but a larger IC than the other solutions. This is achieved by increasing the clearance and the girder height by 29% and the flange width by 10%. Design #3 calls for the lowest IC, but has a failure probability of 0.119. However, this probability refers to a 60-minute functionality performance objective. Furthermore, the time required to evacuate the considered bridge in the event of a fire is expected to be short enough not to endanger the useres' life safety. Hence, Design #3 may still be acceptable from a life-cycle cost perspective, balancing initial material and fire-induced failure costs. Further investigations on this matter are outside the scope of this paper. However, an illustrative example of such an analysis can be found for seismic design in the study by Liu et al. [51].

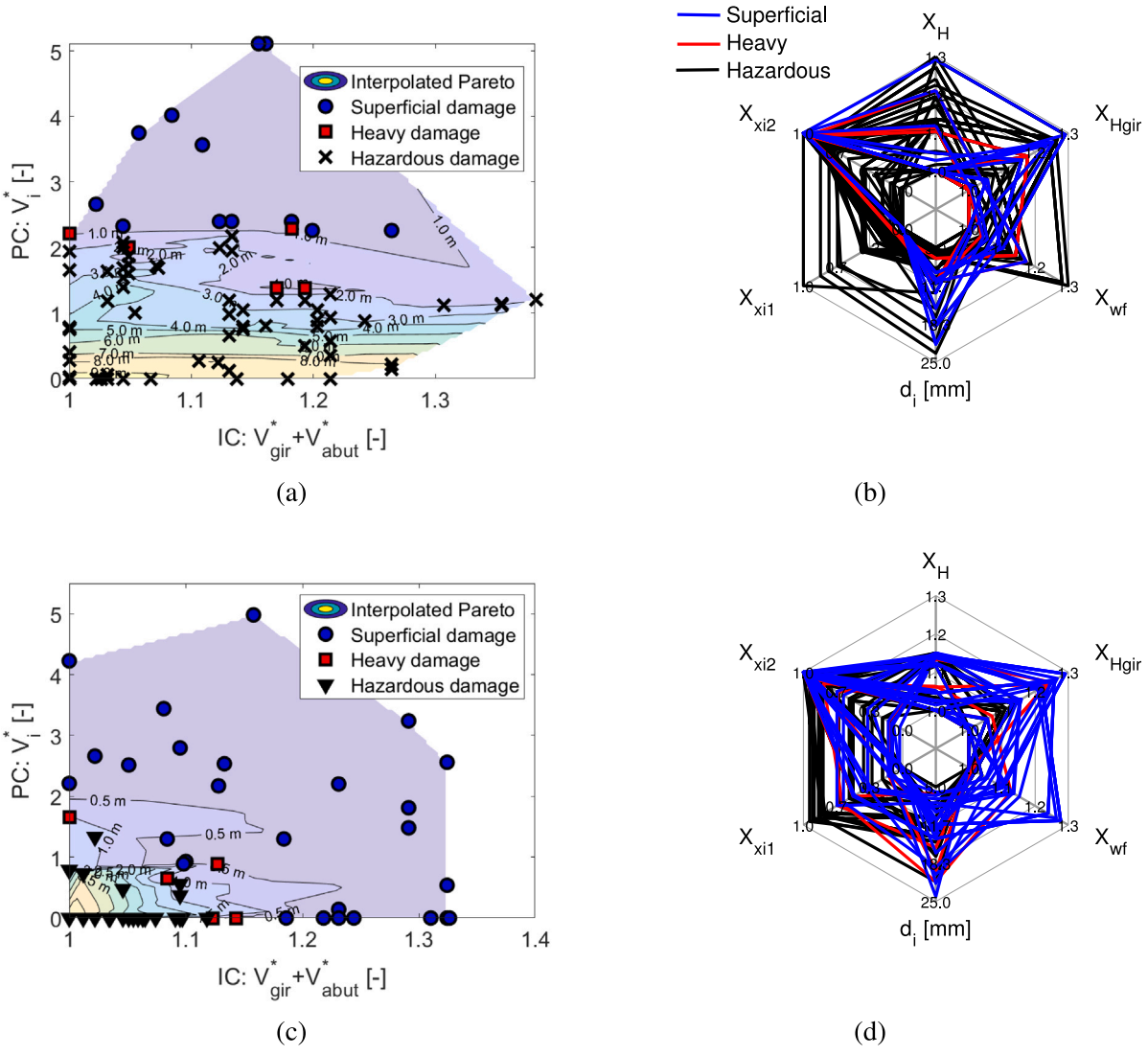

Fig. 8. Optimised design variables and damage states for: (a,b) HGV fire; (c,d) car fire.

Table 3
Selecetd design configurations.

	Design variables $\mathbf{X}^{opt}$						Capacity		Maximum consequence scenario $\boldsymbol{\alpha}_{MC}$				Consequence metrics	
	X_H [–]	X_{Hgir} [–]	X_{wf} [–]	di [mm]	X_{xi1} [–]	X_{xi2} [–]	IC [–]	PC [–]	$\alpha_{bed,MC}$ [–]	$\alpha_{hrrmax,MC}$ [–]	$\alpha_{tmax,MC}$ [–]	$\alpha_{ts,MC}$ [–]	δ_{max} [m]	$1-p_f$ [–]
#1	1.29	1.29	1.10	9.38	0.01	1.00	1.26	2.26	0.20	0.94	1.07	0.51	0.04	0.997
#2	1.03	1.25	1.07	21.88	0.00	0.99	1.16	5.11	0.75	0.93	0.96	0.59	0.03	1.000
#3	1.00	1.02	1.06	11.25	0.00	1.00	1.04	2.33	0.53	0.93	0.96	0.61	0.08	0.881

Table 4
Assumed random material variables and their probability models [50].

Variable	Distribution	Mean	CoV	Units
Yielding stress	Lognormal	281	0.07	MPa
Elastic modulus	Lognormal	210	0.03	GPa
Density	Normal	7850	0.01	kg/m^3

4. Conclusions

This paper introduced the concept of inherent fire capacity, which was then exploited into a structural design optimisation methodology aimed at minimising fire consequences. The following conclusions can be drawn:

- The proposed methodology effectively minimises maximum fire consequences. In doing so, addressing the trade-off between inherent fire capacity (i.e. the capacity of a structure to retain its integrity/functionality without the need for fire safety measures) and passive fire protection enables optimising fire safety designs based on project-specific requirements/performance objectives.
- The design of a simple case study bridge equipped with fire protection measures was optimised using the proposed approach. The structural functionality could be ensured even after 60 min of exposure to a heavy goods vehicle fire.
- The optimisation process generated multiple Pareto-optimal solutions to minimise the maximum bridge deflection (used as a proxy for assessing the bridge damage states and hence its functionality). Fire protection was necessary to achieve the desired functionality objective when facing a heavy goods vehicle fire. On

Table A.1
Considered experimental data.

Data	Context	Data type	Scaling assumptions
#1 [28]	Free flame	Flame centreline excess temperature	$\dot{Q} = 57.5$ kW (max used); $D = 0.3$ m as in the study; $h_c = 35$ W/m^2K; $\varepsilon_f = 1$, $\varepsilon_s = 0.7$, $\phi = 1$
#2 [37]	Free flame (large pool fires)	Flame centreline excess temperature	Same as #1
#3 [38]	Unconfined ceiling	Heat flux at stagnation point $\dot{q}''_s$ vs. H/H_{flame}	–
#4 [39]	Unconfined ceiling	Heat flux at stagnation point $\dot{q}''_s$ vs. $H'_{flame}/(H+y')$	$\dot{Q} = 400$ kW, $H = 1$ m
#5–#8 [38]	Unconfined ceiling	Nondimensional heat flux $\dot{q}''H^2/\dot{Q}$ vs. r/H: #5: $\dot{Q} = 2.9$ kW; #6: $\dot{Q} = 4.0$ kW; #7: $\dot{Q} = 6.3$ kW; #8: $\dot{Q} = 10.5$ kW	For a given $\dot{Q}$, H is calculated to match the maximum heat flux at the stagnation point ($\dot{q}''_s$)
#9 [29]	Unconfined ceiling	Nondimensional heat flux $\dot{q}''H^2/\dot{Q}$ vs. r/H	$\dot{Q}_c = 3.85$ kW (max used); D and H average of the used ones
#10–#13 [42]	Tunnel fire	Heat flux as a function of distance (r) from impingement point: #10: $H = 0.17$ m, $\dot{Q} = 15$ kW; #11: $H = 0.30$ m, $\dot{Q} = 15$ kW; #12: $H = 0.17$ m, $\dot{Q} = 9$ kW; #13: $H = 0.40$ m, $\dot{Q} = 9$ kW	–
#14–#15 [40]	Confined ceiling	Heat flux as a function of dimensionless distance along the flame: #14: $H = 1.1$ m #15: $H = 0.6$ m	$\dot{Q} = 400$ kW (max used); D that provides the same area as the used rectangular burner
#16 [41]	Confined ceiling	Same as #15	Same as #15
#17 [43]	Tunnel fire	Heat flux range	–
#18–#20 [36]	Bridge fire test	Maximum flame centreline and ceiling jet temperatures. #18: $H = 1.85$ m, $\dot{Q} = 426$ kW; #19: $H = 1.85$ m, $\dot{Q} = 1130$ kW; #20: $H = 1.25$ m, $\dot{Q} = 1130$ kW	Data for central deck region. $h_c = 35$ W/m^2K; $\varepsilon_f = 1$, $\varepsilon_s = 0.7$, $\phi = 1$
#21 [44]	Objects immersed in large pool fires	Measured heat flux	–

Symbols: $\dot{Q}$ heat release rate; D burner diameter; h_c convective heat transfer coefficient; ε_f emissivity of the fire; ε_s emissivity of the surface; ϕ configuration factor; H_{flame} mean height of the flame plume; H ceiling height or clearance; r distance from the impingement point; H'_{flame}, y' flame length and virtual source location as defined in Ref. [39,44].

the other hand, several solutions that required fire protection in specific limited girder regions were found in the case of exposure to a car fire.
- The decision-making process benefited from investigating the solutions' robustness to uncertainties in material properties and heat flux model. Failure probabilities for selected Pareto-optimal designs ranged from approximately 0 to 0.119 based on different combinations of fire protection and inherent capacity.

Future research should probabilistically characterise the reliability of fire protection and include it in the analysis. Furthermore, the solutions' robustness to uncertainty and the life-cycle cost/embodied carbon can be included in the performance objectives for optimisation. Finally, it is remarked that the presented case study is purely illustrative (see the limitations discussed in Ref. [7]). Consequently, the proposed methodology should be validated within more realistic structural design contexts.

Declaration of competing interest

The authors declare that they have no known competing financial interests or personal relationships that could have appeared to influence the work reported in this paper.

Data availability

Data will be made available on request.

Acknowledgements

The first author greatly acknowledges the financial support of the Maurice Franses Memorial Trust; the UCL's Department of Civil, Environmental and Geomatic Engineering; and the Society for Fire Protection Engineering through a Student Research Grant as part of the May 2022 Grant Cycle.

Appendix. Experimental heat flux data

Table A.1 summarises the experimental heat flux data used to calibrate the model presented in Section 3.3.2.

References

[1] M.A. Johann, L.D. Albano, R.W. Fitzgerald, B.J. Meacham, Performance-based structural fire safety, J. Perform. Constr. Facil. 20 (1) (2006) 45–53, http://dx.doi.org/10.1061/(ASCE)0887-3828(2006)20:1(45).
[2] S.E. Quiel, T. Yokoyama, L.S. Bregman, K.A. Mueller, S.M. Marjanishvili, A streamlined framework for calculating the response of steel-supported bridges to open-air tanker truck fires, Fire Saf. J. 73 (2015) 63–75.
[3] M. Shrivastava, A. Abu, R. Dhakal, P. Moss, State-of-the-art of probabilistic performance based structural fire engineering, J. Struct. Fire Eng. (2019) http://dx.doi.org/10.1108/JSFE-02-2018-0005.
[4] R. Ma, C. Cui, M. Ma, A. Chen, Performance-based design of bridge structures under vehicle-induced fire accidents: basic framework and a case study, Eng. Struct. 197 (2019) 109390.
[5] J.L. Torero, The risk imposed by fire to buildings and how to address it, in: Protection of Civilian Infrastructure from Acts of Terrorism, Springer, 2006, pp. 41–57.
[6] J.L. Torero, Structures in fire or fires in structures? Assessing the true performance of structures in fire, in: Research and Applications in Structural Engineering, Mechanics and Computation, CRC Press, 2013, pp. 721–722.
[7] A. Franchini, C. Galasso, J.L. Torero, Consequence-oriented fire intensity optimisation for structural design under uncertainty, 2023, submitted for publication in the ASCE Journal of Structural Engineering. Under invited revisions.
[8] A.H. Buchanan, A.K. Abu, Structural Design for Fire Safety, John Wiley & Sons, 2017.
[9] A. Jowsey, P. Scott, J.L. Torero, Overview of the benefits of structural fire engineering, Int. J. High-Rise Build. 2 (2) (2013) 131–139.
[10] J. Hu, R. Carvel, A. Usmani, Bridge fires in the 21st century: A literature review, Fire Saf. J. 126 (2021) 103487.
[11] Highway Agency, Highway agency initial fire risk audit report, 2011, https://assets.publishing.service.gov.uk/government/uploads/system/uploads/attachment_data/file/360251/ha-initial-fire-risk-audit-report.pdf.
[12] J.A. Purkiss, L.-Y. Li, Fire Safety Engineering Design of Structures, CRC Press, 2013.
[13] C.G. Bailey, G.M. Newman, J. Robinson, Fire Safe Design: A New Approach to Multi-Storey Steel-Framed Buildings, Steel Construction Institute, Ascot, U.K., 2006.
[14] T.A. Kletz, P. Amyotte, Process Plants: A Handbook for Inherently Safer Design, Crc Press, 2010.
[15] J.E. Cadena, M. McLaggan, A.F. Osorio, J.L. Torero, D. Lange, Maximum allowable damage approach to fire safety performance quantification, Fire Saf. J. 128 (2022) 103537.
[16] M.J. Hurley, E.R. Rosenbaum, Performance-based design, in: SFPE Handbook of Fire Protection Engineering, Springer, 2016, pp. 1233–1261.
[17] C. Kirchsteiger, On the use of probabilistic and deterministic methods in risk analysis, J. Loss Prev. Process Ind. 12 (5) (1999) 399–419.

[18] M.E. Paté-Cornell, Uncertainties in risk analysis: Six levels of treatment, Reliab. Eng. Syst. Saf. 54 (2–3) (1996) 95–111.
[19] M.J. Hurley, D.T. Gottuk, J.R. Jr. Hall, K. Harada, E.D. Kuligowski, M. Puchovsky, J.L Torero, J.M. Jr. Watts, C. Wieczorek, SFPE Handbook of Fire Protection Engineering, Springer, 2016.
[20] G. Peris-Sayol, I. Paya-Zaforteza, J. Alos-Moya, A. Hospitaler, Analysis of the influence of structural models in fire responses of steel girder bridges, in: Structures Congress 2015, 2015, pp. 160–171, http://dx.doi.org/10.1061/9780784479117.014.
[21] EN 1991-2. Eurocode 1: Actions on structures - Part 2: Traffic loads on bridges, European Committee for Standardization, 2003.
[22] I. Payá-Zaforteza, M.E.M. Garlock, A numerical investigation on the fire response of a steel girder bridge, J. Construct. Steel Res. 75 (2012) 93–103.
[23] H. Ingason, A. Lönnermark, Heat release rates from heavy goods vehicle trailer fires in tunnels, Fire Saf. J. 40 (7) (2005) 646–668.
[24] NFPA-502, Standard for Road Tunnels, Bridges, and Other Limited Access Highways, NFPA, 2011.
[25] CETU, Guide Dossiers Sécurité - Les études Spécifiques des Dangers, CETU, 2003, https://www.cetu.developpement-durable.gouv.fr/IMG/pdf/Guide_dossier_securite-Fasc_4_cle0e377a.pdf.
[26] M.Z. Mohd Tohir, M. Spearpoint, Distribution analysis of the fire severity characteristics of single passenger road vehicles using heat release rate data, Fire Sci. Rev. 2 (1) (2013) 1–26, http://dx.doi.org/10.1186/2193-0414-2-5.
[27] D. Drysdale, An Introduction to Fire Dynamics, John Wiley & Sons, 2011.
[28] B.J. McCaffrey, Purely buoyant diffusion flames: some experimental results, NBSIR 79-1910, Center for Fire Research, Washington, D.C., 1979.
[29] H.Z. You, G.M. Faeth, Ceiling heat transfer during fire plume and fire impingement, Fire Mater. 3 (3) (1979) 140–147.
[30] G. Heskestad, Fire plumes, flame height, and air entrainment, SFPE Handb. Fire Protect. Eng. (2016) 396–428.
[31] G. Cox, R. Chitty, A study of the deterministic properties of unbounded fire plumes, Combust. Flame 39 (2) (1980) 191–209.
[32] G. Heskestad, Luminous heights of turbulent diffusion flames, Fire Saf. J. 5 (2) (1983) 103–108.
[33] R.L. Alpert, Ceiling jet flows, SFPE Handb. Fire Protect. Eng. (2016) 429–454.
[34] C.L. Beyler, Fire hazard calculations for large, open hydrocarbon fires, SFPE Handb. Fire Protect. Eng. (2016) 2591–2663.
[35] J. Alos-Moya, I. Paya-Zaforteza, A. Hospitaler, P. Rinaudo, Valencia bridge fire tests: Experimental study of a composite bridge under fire, J. Construct. Steel Res. 138 (2017) 538–554.
[36] J. Alos-Moya, I. Paya-Zaforteza, A. Hospitaler, E. Loma-Ossorio, Valencia bridge fire tests: Validation of simplified and advanced numerical approaches to model bridge fire scenarios, Adv. Eng. Softw. 128 (2019) 55–68.
[37] H.R. Baum, B.J. McCaffrey, Fire induced flow field-theory and experiment, Fire Saf. Sci. 2 (1989) 129–148.
[38] M.A. Kokkala, Experimental study of heat transfer to ceiling from an impinging diffusion flame, in: Fire Safety Science—Proceedings of the Third International Symposium, Routledge, 2006, pp. 261–270, https://publications.iafss.org/publications/fss/3/261.
[39] Y. Hasemi, S. Yokobayashi, T. Wakamatsu, A. Ptchelintsev, Fire safety of building components exposed to a localized fire: Scope and experiments on ceiling/beam system exposed to a localized fire, in: Proceedings of ASIAFLAM, 1995, pp. 351–361.
[40] B.Y. Lattimer, C. Mealy, J. Beitel, Heat fluxes and flame lengths from fires under ceilings, Fire Technol. 49 (2013) 269–291.
[41] P. Hinkley, H.G.H. Wraight, C.R. Theobald, The contribution of flames under ceilings to fire spread in compartments part I incombustible ceilings, Fire Res. Not. 712 (1968) https://publications.iafss.org/publications/frn/712/-1.
[42] L. Chen, F. Tang, H. Pang, Ceiling heat flux and downward received radiation heat flux induced by weak and relative strong fire plume in ventilation tunnels, Appl. Therm. Eng. 169 (2020) 114924.
[43] T. Shaw, T. Gibson, J. Karlovšek, R. Emberley, J.L. Torero, Experimental evaluation of the heat flux induced by tunnel fires, Tunnel. Undergr. Space Technol. 60 (2016) 49–55.
[44] B.Y. Lattimer, Heat transfer from fires to surfaces, SFPE Handb. Fire Protect. Eng. (2016) 745–798.
[45] L.T. Cowley, Behaviour of oil and gas fires in the presence of confinement and obstacles, Steel Construction Institute, Ascot, U.K., 1992.
[46] A.M. Sanad, S. Lamont, A.S. Usmani, J.M. Rotter, Structural behaviour in fire compartment under different heating regimes–part 2: (slab mean temperatures), Fire Safety Journal 35 (2) (2000) 117–130, http://dx.doi.org/10.1016/S0379-7112(00)00025-4.
[47] J. Jiang, L. Jiang, P. Kotsovinos, J. Zhang, A. Usmani, F. McKenna, G.-Q. Li, OpenSees software architecture for the analysis of structures in fire, J. Comput. Civ. Eng. 29 (1) (2015) 04014030, http://dx.doi.org/10.1061/(ASCE)CP.1943-5487.0000305.
[48] EN 1993-1-2. Eurocode 3: Design of steel structures - Part 1-2: General rules - Structural fire design, 2005.
[49] M. Awad, R. Khanna, Efficient learning machines: theories, concepts, and applications for engineers and system designers, Springer nature, 2015, http://dx.doi.org/10.1007/978-1-4302-5990-9.
[50] S. Devaney, Development of Software for Reliability Based Design of Steel Framed Structures in Fire (Ph.D. dissertation), University of Edinburgh, 2015, https://era.ed.ac.uk/handle/1842/10468.
[51] M. Liu, S.A. Burns, Y.K. Wen, Optimal seismic design of steel frame buildings based on life cycle cost considerations, Earthquake engineering & structural dynamics 32 (9) (2003) 1313–1332, http://dx.doi.org/10.1002/eqe.273.